The Iowa Cyclonic-Anticyclonic Tornado Pair and Its Parent Thunderstorm

JOHN M. BROWN

Office of Weather Research and Modification, NOAA, Boulder, CO 80303

KEVIN R. KNUPP

Department of Atmospheric Science, Colorado State University, Fort Collins 80523

(Manuscript received 13 August 1979, in final form 23 June 1980)

ABSTRACT

A severe thunderstorm which spawned at least four tornadoes, one of them anticyclonic, formed over central Iowa during the afternoon of 13 June 1976. This storm moved toward the east-northeast, approximately parallel to but slower than the mean tropospheric flow. The anticyclonic tornado (F3) and the most intense (F5) of the cyclonic tornadoes coexisted for 25 min and traveled on nearly parallel, cycloidal-like tracks, with the anticyclonic tornado 3–5 km southeast of the cyclonic. The major emphasis of this paper is on this pair of tornadoes and their relationship to the structure and evolution of the parent thunderstorm.

Radar recorded the development of a hook echo just prior to the genesis of the intense cyclonic tornado. A strengthening mesolow was centered somewhere south of this tornado soon after it formed. The mesolow is believed to have initiated a new updraft; the anticyclonic tornado formed in association with this updraft, south of the cyclonic tornado. It is hypothesized that the mesolow was responsible (through alteration of the storm-scale airflow) for the nearly simultaneous sharp right turns made by these tornadoes. Each of these tornadoes was observed to diminish in intensity soon after becoming associated with heavy rain.

It is argued that the parent thunderstorm's distinctive airflow and thermodynamic structure at low levels provided a more favorable setting for the amplification of anticyclonic vorticity than is typical of most severe thunderstorms.

1. Introduction

On 13 June 1976 the authors had the good fortune to witness a particularly awesome Iowa thunderstorm having supercell (Marwitz, 1972) characteristics. Subsequent analysis of a variety of data has convinced us that this event had several unique or distinctive features worthy of reporting, specifically the following:

1) The occurrence of an anticyclonic tornado, well documented by excellent movie footage[1].

2) The extreme (F5) intensity of one of the cyclonic tornadoes.

3) The parallel, cycloid-like tracks of the anticyclonic tornado (designated T3) and the intense cyclonic tornado (T2).

4) Passage of both the anticyclonic and intense cyclonic tornadoes through a dense rain-gage network.

In this paper we concentrate on the relationship of the tornadoes to the structure and evolution of the parent thunderstorm. A more detailed discussion of some aspects of this case can be found in Brown.[2] Fujita (1977, 1978[3]), and Fujita and G. S. Forbes (1979, personal communication) have carried out an independent investigation of this event.

2. Data sources

Conventional data obtained for this study include hourly surface aviation weather reports, radiosonde observations, visible and infrared geostationary satellite photos, and the WSR-57 radarscope film record taken at the Des Moines (DSM) National Weather Service Forecast Office.

A color densitometer at the National Hurricane and Experimental Meteorology Laboratory, Coral Gables, Florida, was used to examine the film record. This device, which resolves the brightness (proportional to returned signal intensity) of the (photographed) scope presentation into colors, confirmed a great deal of structure to the radar echo which was only vaguely apparent to the eye from study of the projected black and white frames.

[1] Mr. Charles Barthold provided exceptional coverage ("Central Iowa Tornadoes, June 13, 1976." Copyright Palmer Broadcasting Company, Des Moines).

[2] Brown, J. M., 1979: Central Iowa tornado family, 13 June 1976. Final Report to National Severe Storms Laboratory. Grant 01-7-022-13204 to Iowa State University, 132 pp. [Available from author, U.S. Department of Commerce, NOAA, ERL, Rx8, 325 Broadway, Boulder, CO. 80303].

[3] Fujita, T. T., 1978: Manual of downburst identification for Project NIMROD. SMRP Res. Pap. No. 156, Dept. Geophys. Sci., The University of Chicago. 104 pp. [NTIS PB-286 048/4G1].

0027-0644/80/101626-21$09.25

A ground-based damage survey of the tornado-stricken area was conducted from 15 to 22 June 1976. A cursory aerial survey was made on 15 June 1976. Numerous eyewitnesses were interviewed in June, July and August. The return of 120 questionnaires distributed in September 1976 provided information concerning the tornadoes and associated weather. The analysis of ~300 photographs and eight movie films provided information on tornado-funnel shapes, sizes, translational speeds, cloud and precipitation patterns and surface wind estimates in the vicinity of the tornadoes.

The two tornadoes of major interest (T2 and T3) fortuitously passed through a network of 22 recording rain gages (operated by the Agricultural Experiment Station of Iowa State University) laid out on a 1 statute mile (1.6 km) grid. Time resolution of the rain-gage charts was ~1 min. The charts were changed about 3–4 h prior to the passage of the tornadoes; the "time on" of the charts was recorded using a watch synchronized with a universal time standard. Chart rates were also accurately determined for each gage, so that with corrections applied, the timing of nearly all charts is considered accurate to ±1–2 min.

3. Meso-α scale[4] environment and thunderstorm beginnings

The synoptic situation at 1200 GMT 13 June 1976 is summarized in Fig. 1. The front, oriented south-southwest to north-northeast, marks the surface boundary between convectively unstable marine tropical air to its east and slightly cooler and much drier Pacific air to the west, modified considerably by travel across the western United States. The diffuse stationary front over north central Iowa and southern Minnesota extends northeastward to an occluded front and intense low in southern Canada. The weak low in western Kansas moved northeastward slowly during the day and by 1200 CST was located in south-central Nebraska. There was appreciable warm advection to the east of this low as evidenced by the veering winds between 850 and 500 mb (Fig. 1), and the stationary front across Iowa receded slowly northward as a warm front during the morning and early afternoon on 13 June. Dewpoints in central Iowa steadily increased until mid-afternoon, rising in Des Moines from 17°C at 1200 GMT to 23°C at 1900.

Ingredients for occurrence of severe thunderstorms over the Midwest, namely, strong vertical shear of the horizontal wind, strong convective instability (as evidenced by the decrease in equivalent potential temperature with height) in the lower troposphere, and a mechanism for upward motion on a synoptic or smaller scale (in this case, warm advection at lower levels), were present during the day of 13 June over much of Iowa, northwest Missouri and southeast Nebraska. The extreme potential buoyant energy that built up over the area during the morning of 13 June is shown by Fig. 2a, a sounding constructed for central Iowa at 1900 GMT, about the time this energy began to be explosively released. The boundary-layer portion of this sounding accepts the DSM surface temperature and dewpoint as lower boundary values. These are extrapolated upward with height, incorporating a superadiabatic surface layer in which the potential temperature and the dewpoint decrease with height. This is surmounted by a well-mixed layer having nearly constant potential temperature and mixing ratio. The percentage falloff of mixing ratio in the surface layer is consistent with that noted by Johnson (1977) in the landbased mixed layer over south Florida and by Steyaert and Darkow[5] in moist southerly flow situations during May and June at Columbia, Missouri. The scattered stratocumulus (Sc) stratiformis cumulomutatus and Sc lenticularis cumulomutatus observed over central Iowa during the early afternoon argue for a mixing ratio averaging near but less than saturation near the top of the mixed layer.

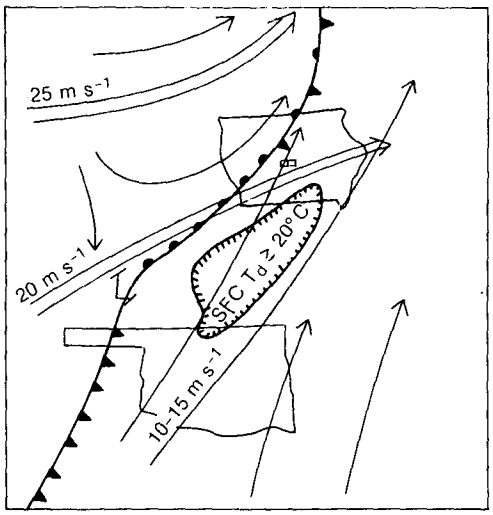

FIG. 1. Major map features near 1200 GMT 13 June 1976. Single arrows indicate low-level wind flow. Double arrows depict airflow at 500 mb. The two small squares in central Iowa outline Boone and Story counties. A region of surface dewpoints (T_d) ≥ 20°C is indicated extending southwestward from south central Iowa.

[4] We adopt the length-scale conventions: meso-α = 250–2500 km, meso-β = 25–250 km, meso-γ = 2.5–25 km (Orlanski, 1975).

[5] Steyaert, L. T., and G. L. Darkow, 1973: Diurnal variations in the ability to infer spatial variability in the thermodynamic properties of the lowest kilometer from surface data. *Preprints 8th Conf. Severe Local Storms*, Denver, Amer. Meteor. Soc., 238–243.

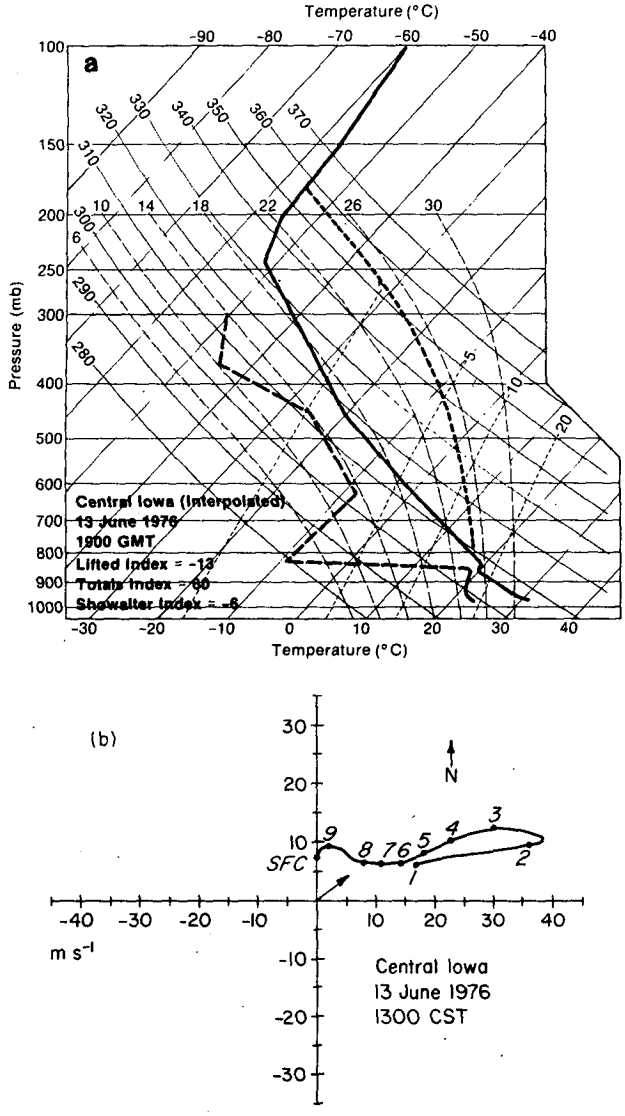

FIG. 2. Interpolated environmental conditions over central Iowa at 1900 GMT 13 June 1976, near the time of formation of the parent thunderstorm. (a) Skew T–log$P$ plot of temperature and dewpoint. The wet adiabat (θ_w = 24.8°C) corresponding to mean conditions in the subcloud layer is shown. (b) Wind hodograph: The abscissa and ordinate are the u and v wind components, respectively, and the numbers in italics indicate pressure in hundreds of millibars; SFC indicates the surface wind. The small arrow emanating from the origin indicates the motion of the centroid of the high-reflectivity portion of the radar echo during the tornadic activity.

The sounding structure above the mixed layer is obtained by estimating the potential temperature at the 1200 GMT position of isentropic, isobaric trajectories above 850 mb which terminate over central Iowa at 1900. The absence of moist convection above 850 mb upstream from Iowa argues in favor of the isentropic assumption. There results a very minor inversion near 850 mb topping the mixed layer, consistent with the observed Sc. This suggests that the assumption of no vertical motion is satisfactory. (In any event, the sounding at the low levels above the mixed layer is insensitive to assumed vertical motion because the lapse rate is close to dry adiabatic.)

Parcel-method vertical velocity for a parcel with mean mixed-layer properties [wet-bulb potential temperature θ_w = 24.8°C (see Fig. 2a)] reaches 98 m s^{-1} at the neutral buoyancy level of 178 mb!

The storm which is the subject of this study was first sighted by one of us (KK) near 1850 GMT ~60 km west of DSM while still a cumulus congestus. Shortly afterward a second cumulus congestus became visible just south of the first. For several minutes after these clouds first clearly exhibited glaciated tops the DSM WSR-57 detected no echo at 0.5° elevation, indicating that the level of first echo was above 2 km. These adjoining clouds had separate radar echoes initially, but before 2000 the echoes merged at low reflectivity. Large hail fell north of Ogden (see Fig. 3 for location) about 1940 marking the first known report of severe weather.

At 1956 the touchdown of the first tornado (from the southern member of the cloud and echo pair mentioned above) marked the beginning of the tornadic activity which continued for the next 1.5 h. The overall storm motion between 2000 and 2100 GMT was to the east-northeast to northeast, slower and similar in direction to the mass-averaged tropospheric flow but strongly to the right of the ambient flow in the low-level moist layer (Fig. 2b). This favored the southern member of the cloud pair; the northern member lost identity after 2000.

This was the first and most intense of several severe thunderstorms which had developed by 2100 in a wide band running from just west of Omaha to near Waterloo. Many occurrences of strong winds and very large hail were reported after 2100 over the southeast two-thirds of Iowa. By 2200, several individual severe thunderstorms had interacted over southwest and central Iowa to form a southeastward moving squall line which persisted past midnight.

4. Chronology of events

The parent thunderstorm of the 13 June central Iowa tornado family spawned four tornadoes. In addition, substantial straight-line wind damage occurred and several funnel clouds were reported. The best estimate of the tornado time-track history as determined from our damage survey, eyewitness reports and analysis of photos, is shown in Fig. 3 along with approximate F-scale intensity.[6] Table 1

[6] Fujita, T. T., 1971: Proposed characterization of tornadoes and hurricanes by area and intensity. SMRP Res. Pap. No. 91, Dept. Geophys. Sci., The University of Chicago, 42 pp. [NTIS COM-72-10828].

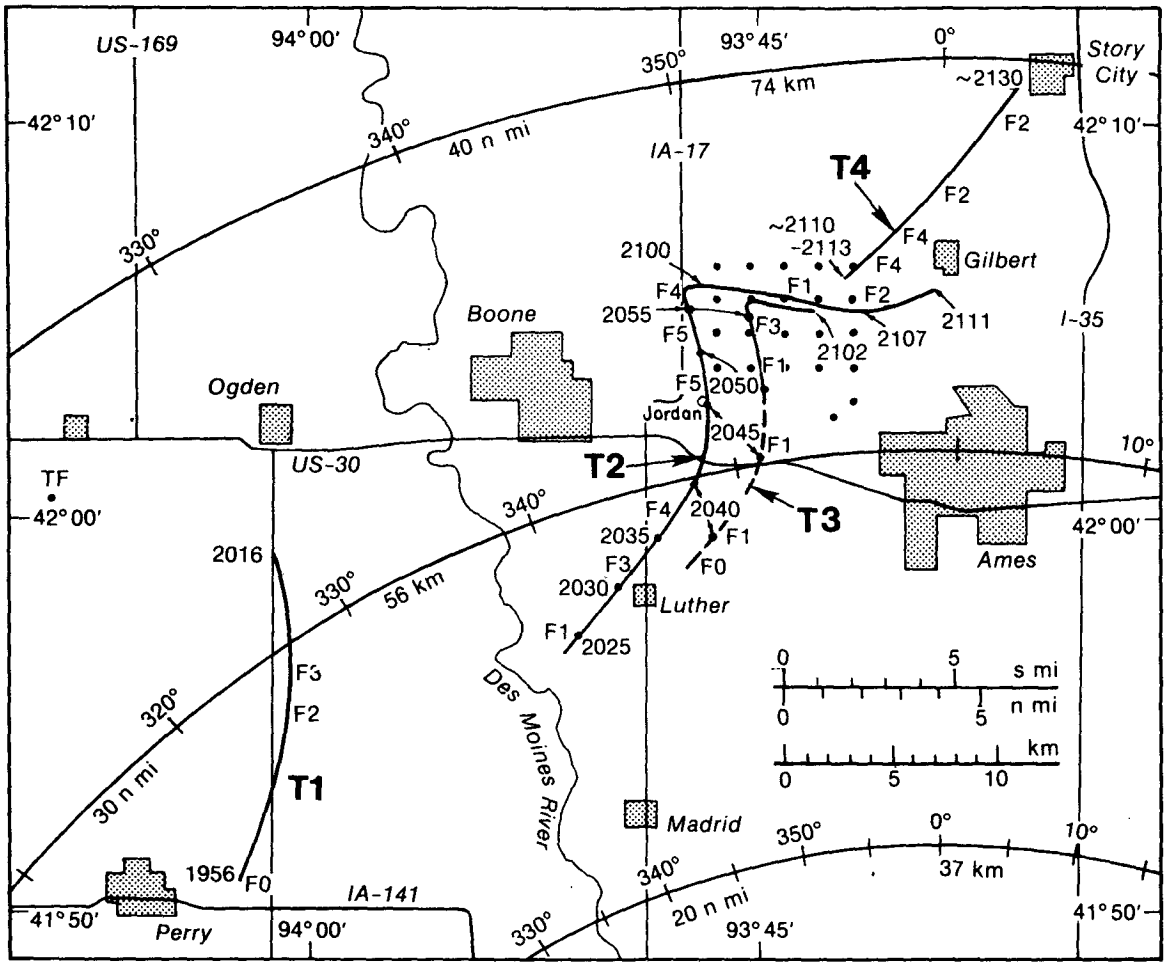

FIG. 3. Time-track-intensity history of tornadoes occurring in central Iowa on 13 June 1976. Times are GMT and more tentative segments of the tracks are dashed. F-scale intensity levels are approximate. On this and later figures range and azimuth from the WSR-57 radar at Des Moines (DSM) are shown, as are geographic landmarks. The matrix of dots, also shown on later figures, is the rain-gage network through which T2 and T3 passed.

provides additional information concerning the tornadoes.

a. Storm evolution and description of events before 2100 GMT

Events while the tornadoes were in existence are now described. In discussing the radar-echo structure we emphasize the period 2000–2104 when the radarscope photography is at 50 n mi (93 km) range. Fig. 4 depicts the shades of gray which appear on the radar pictures (processed by densitometer) discussed below. The "brightest" echoes (strongest returned signal) correspond to the left of this figure and echo-free areas to the extreme right.

Fig. 5 is a display of 18 selected scans between 2009 and 2104. The locations of the 30 n mi (56 km) and 40 n mi (74 km) range marks (faintly visible as white arcs in some scans) are denoted by the black number 3 or 4 on the photographs, and azimuths (tens of degrees) are labeled near the top of each photo. The points of the small markers

TABLE 1. Statistics on the 13 June 1976 central Iowa tornadoes.

	Tornado			
	1	2	3†	4
Formation (GMT)	1956*	2023*	2036*	2111**
Dissipation (GMT)	2016*	2111*	2102*	2130**
Duration (min)	20	48	26	19
Maximum width of damage path (km)	0.4	1.5	0.8	5
Path length (km)	16	34	16	13
Maximum intensity	F3	F5	F3	F4
Rotation	cyclonic	cyclonic	anticyclonic	cyclonic
Average translational speed (m s^{-1})	13.0	11.8	10.5	11.1

* Possible error of 3 min.
** Possible error of 5 min.
† Assumes T3 formed 2–3 km northeast of Luther.

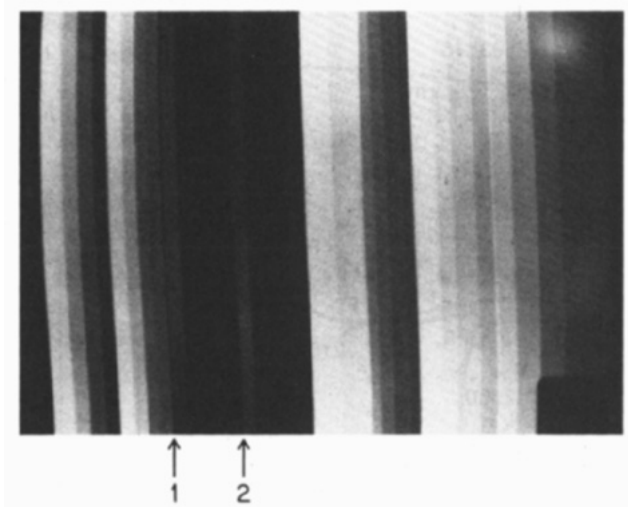

FIG. 4. Shades of gray appearing in the radar pictures of Fig. 5. Strongest returned signal ("brightest" echo) corresponds to the extreme left of this figure, echo-free areas to the extreme right. The white-to-black transition (going right to left, near the center of this figure) is very prominent on the Fig. 5 radar photos. Vertical arrows labeled 1 and 2 indicate the position of color transitions corresponding to radar echo outlines in Figs. 6, 7 and 18.

labeled 1 or 2 on individual photos indicate the position of T1 or T2. The position of T3 on each photo can be inferred from T2's position and the location of T3 relative to T2 on Fig. 3. The placement of radar coordinates with respect to topographic landmarks and the tornado tracks is shown on Fig. 3. Contours of gray on Fig. 5 do not represent the same reflectivity values on each scan but do portray qualitatively regions of high reflectivity and large reflectivity gradient. On many of the scans a discontinuity which marks the start-stop azimuth for the scope camera appears along the 340° radial. Because synchronization is not precise, nil exposure or double exposure is sometimes apparent, rendering unreliable the portrayal of features along this radial.

Tornado 1 (T1) achieved F3 intensity. Events surrounding the formation of T1 are obscure. It likely formed within an updraft-associated mesocyclone, but well away from any sharp discontinuity or boundary separating updraft and downdraft air. Eyewitness reports and photographs indicate that any such boundary was located well north of T1 and probably north of U.S. Highway 30 (Fig. 3) during most of T1's life. T1 exhibited a life cycle closely resembling that of the Union City, Oklahoma tornado described by Golden and Purcell (1978). When first observed it was a surface dust whirl below a bowl-shaped protrusion at cloud base; soon afterward a vertical-axis condensation funnel descended to the surface. This funnel took on the shape of an inverted cone and later achieved a maximum diameter at cloud base of 300 m. T1's condensation funnel narrowed into a contorted ropelike form before dissipating about 2016 GMT.

The low-elevation, zero-attenuation scans at 2009 and 2015 in Fig. 5 show the elliptically shaped echo of the severe thunderstorm north-northwest of DSM. These photos, and earlier ones not presented, do not reveal any prominent echo features that can be associated with T1, which was near the southwest edge of the radar echo at 2009 and 2015 (see Fig. 5; at 2009 GMT T1 is near the upper right corner of the 3 range-mark tab).

A photo taken by T. Fisher from west-southwest of Ogden (point TF on Fig. 3) revealed that T1 was associated with two remarkable cloud bands. A plan view of these bands at 2009.5 is depicted in Fig. 6. Superimposed on this sketch is the outline of transition 1 (Fig. 4) of the 2009 radar echo in Fig. 5 showing a developing finger H (also labeled in Fig. 5). At this time the radar echo was well north of the cloud band. The expanding, lowering base or wall cloud (B, Fig. 6; subsequently the wall cloud of T2), ~6 km in diameter, was clearly visible in several photos taken of T1 (see Brown).[2] After 2010 the middle portion of the band extending southeast from T1 broke up, and the spiral organization of the clouds near T1 disappeared as the cloud base B continued to lower and move northeast. By 2015, just before T1's demise, an echo-free region (Fig. 5) had developed along the Des Moines River north to the latitude of Luther, leaving a pronounced echo appendage near H in Fig. 6 (see Fig. 5). The cloud base B is still believed to have been entirely echo-free at this time. Fig. 5 shows that the echo finger became more hooklike by 2017 and a brief fall of hail 10–15 mm in diameter was observed by Mr. F. Stumbo (point FS, Fig. 6) about 2020 GMT, underneath the radar hook. Shortly after 2020, Stumbo took brief movie footage of a region of cyclonically rotating cloud elements which passed over or just south of his location. Later footage taken by Stumbo shows that T2 first appeared about 2023 in the vicinity of a strong updraft as a slender funnel extending southward and downward from the northern portion of cloud base B.

Fig. 7 depicts the interpolated location of cloud base B (now T2's wall cloud) and the transition 1 echo outline (Fig. 4) at 2025. By this time the zero-elevation radar hook partially intersected the wall cloud, having moved east-northeast while the wall cloud was moving northeast. This wall-cloud motion was nearly parallel to the mid-tropospheric flow, by contrast to the right-moving character of similar features reported by Browning (1965).

We suspect that by 2010 a strong updraft with foot at cloud base B had become established. The development of a wall cloud is indicative of lowering of the lifted condensation level of ascending air

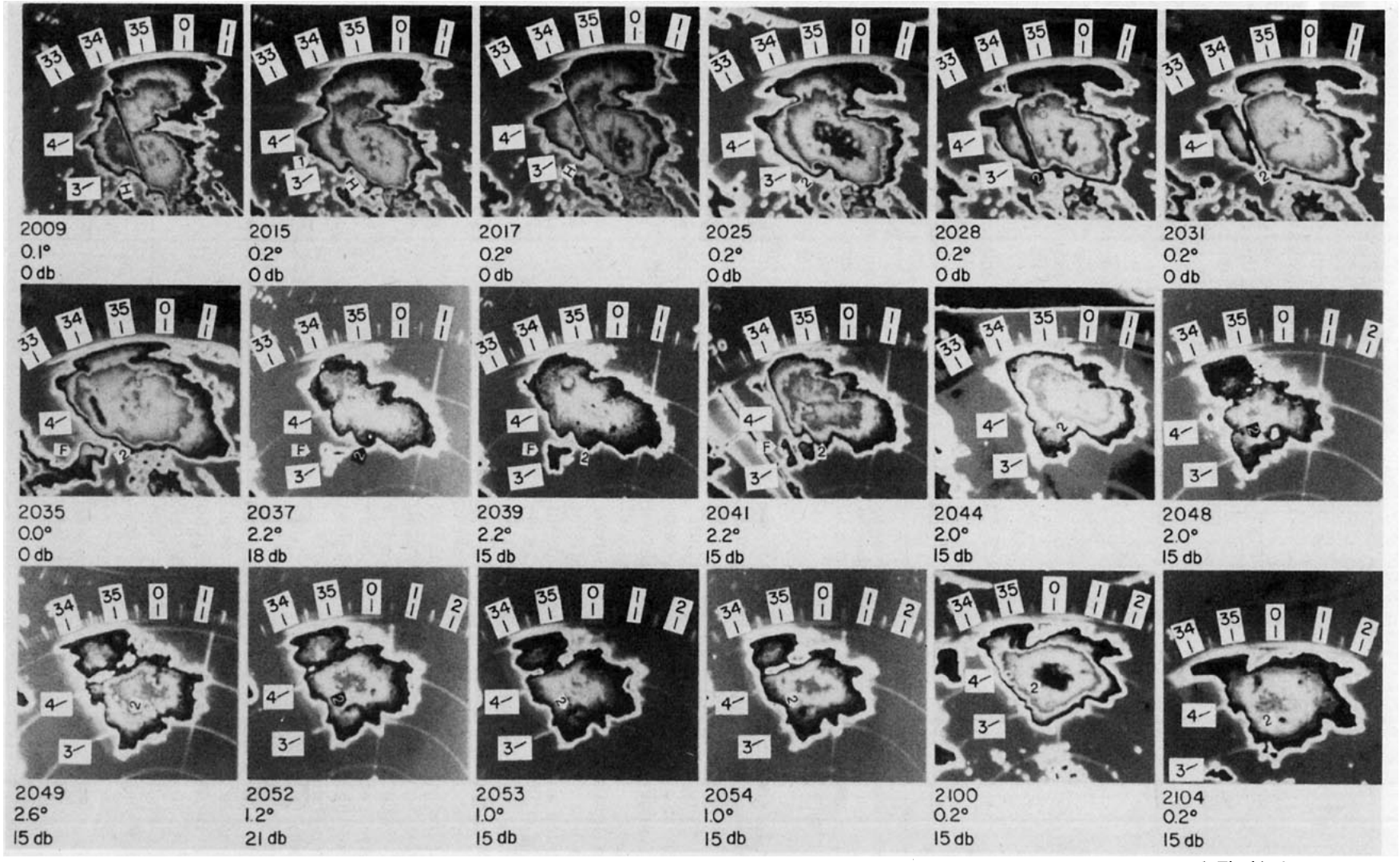

FIG. 5. A series of black and white copies of color densitometer photos, made from a 16 mm copy of the DSM WSR-57 radarscope record. The black numbers 33–35 and 0–2 are azimuths in tens of degrees. The black numbers 3 and 4 indicate positions of the 30 n mi (56 km) and 40 n mi (74 km) range marks, respectively. (These can be seen as faint white arcs on some of the photos.) The labeled markers 1 and 2 denote locations of T1 and T2, respectively. Markers H and F refer to echo features discussed in the text. Time (GMT), elevation angle and attenuation are given just below lower left corner of each photo. Fig. 4 shows the qualitative relationship between reflectivity and shades of gray in these photos. The black splotchy area inside the main echo at 2017, 2025, 2031 and 2100 GMT corresponds to the black (saturation) at the extreme left side of Fig. 4.

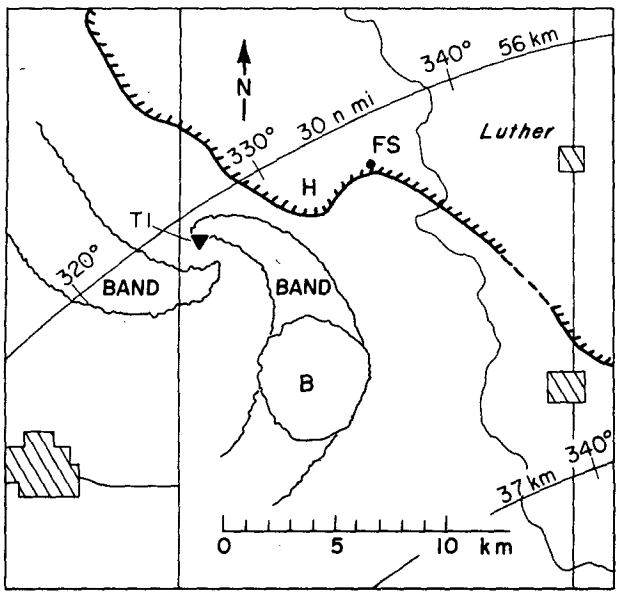

FIG. 6. Outline of cloud bands associated with T1 (indicated by black triangle) and southwest edge of DSM WSR-57 radar echo (transition 1, Fig. 4) at 2009 GMT. Location FS and radar echo feature H are discussed in text.

and often precedes formation of tornadoes that occur in association with an updraft mesocyclone (Davies-Jones, 1978). In the Union City, Oklahoma storm a Doppler-radar tornado-vortex signature (TVS) appeared at middle levels before the wall cloud formed (Golden and Purcell, 1978). Brown *et al.* (1978) claim that a TVS is often detected well before tornado formation, indicating that strong rotation occurs first at mid levels. On the basis of these observations and in view of the subsequent development of T2, a strong counterclockwise swirl was likely developing within the updraft by 2010 GMT. Horizontal vortex lines with a northerly component, associated with westerly vertical shear within and near the top of the moist layer (Fig. 2b), conceivably were being tilted toward the vertical, then stretched within the updraft, to produce this counterclockwise swirl. The hook echo, initially north of T2, most likely resulted from the spiraling trajectory of hail falling through weaker parts of the rotating updraft.

The well-formed hook at 2025 appears to have wrapped completely around the "weak echo region"[7] (WER) by 2028 as the whole feature translated northeast. By 2035 the "bounded weak echo region" (BWER) so formed had completely disappeared at 0° elevation, there being an echo lobe in this position. Rain-gage records (Brown)[2], photographs of T2 taken from within and close to the rain-gage network and eyewitness reports from near Gilbert and points southwest indicate that an area north and east of the hook and T2, where reflectivity was high, received hail up to 35 mm in diameter and significant rain during this period.

The sequence of scans near 2° elevation (Fig. 5) shows that aloft (beam centered at ~2 km near the southern flank of our storm) a very small BWER is evident over the lobe near the surface at 2035. This had filled in by 2041, but the notch or weak echo region to its east near 354° at 31 n mi (57 km) persisted and moved eastward rapidly, to be near 004° at 31 n mi (57 km) at 2049. Evidently, this feature had vertical continuity below 2 km; it appears on later scans at 1° and 0.2° (Fig. 5).

Meanwhile, a new echo, first unambiguously apparent at 2035 GMT (indicated by the pointer labeled F on Fig. 5), merged with the main storm between 2040 and 2044. This echo appears to have moved from ~240° at 25 m s^{-1} between 2035 and 2044, much faster motion than any of the principal storms on this day, and intensified rapidly as it merged with the main storm. It may have been visible as an area of rain falling to the west of T2 near 2040, as photographed by a few eyewitnesses just west of Ames. There is insufficient information to ascertain whether this might be related to the "flanking-line" echo features discussed by Lemon (1976). A result of the merger of this echo with the main storm was the formation of a spectacular BWER, visible at

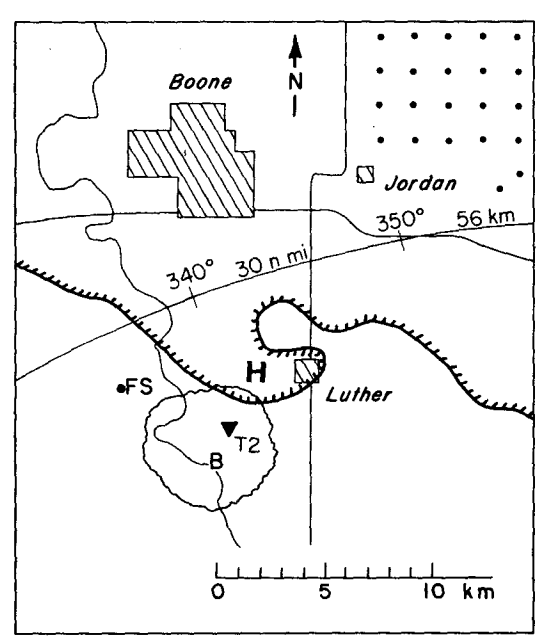

FIG. 7. Outline of T2's wall cloud (T2's position indicated by black triangle) and southwest edge of DSM WSR 57 radar echo (transition 1, Fig. 4) at 2024 GMT. Location FS and radar echo feature H are discussed in text.

[7] There exists no information concerning possible echo overhang over the region of weak echo harbored by the hook (say, at 2025 GMT), so whether this is a true WER possessing echo overhang is not clear.

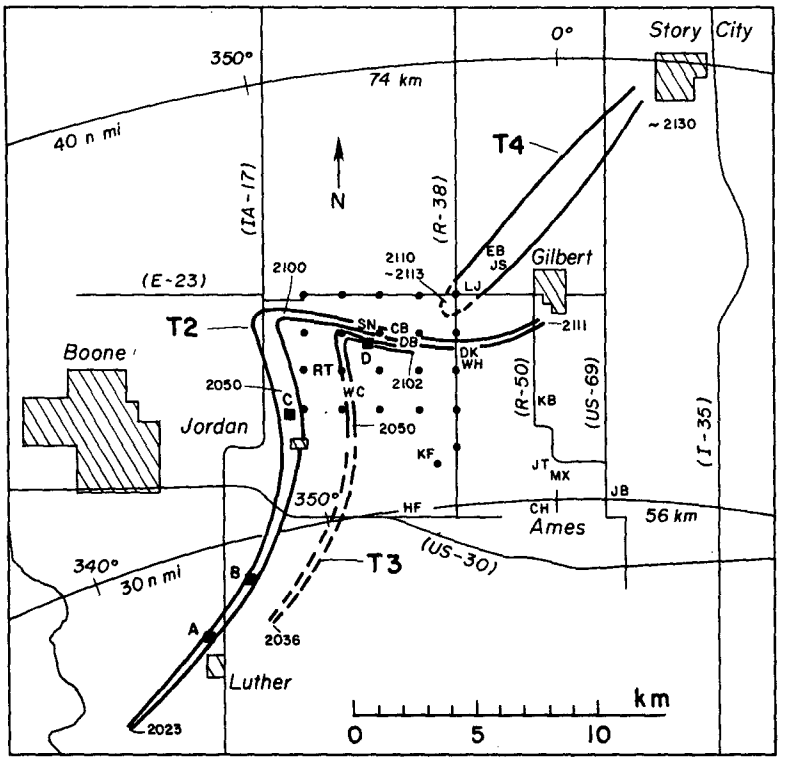

FIG. 8. Location identifiers and time-track history of T2, T3 and T4 as in Fig. 3. T2 underwent marked fluctuations in funnel diameter between points A and B. Points C and D mark the location of T2 and T3, respectively, in the photos shown in Figs. 9 and 11. Microbarographs were operating at locations KF, CH and JB. Other two-letter identifiers mark the locations of eyewitness reports or damage discussed in text.

2048 near 356° at 33 n mi (61 km), east of both T2 and T3. This weakened rapidly by 2049, near 355° at 34 n mi (63 km). After this merger took place, T2 was well within the high reflectivity region at 2° elevation.

A sequence of three scans at 1° elevation are among the most intriguing on Fig. 5. At 2052, a hook is evident at relatively high reflectivity, with a weak BWER ("black hole") just southeast of T2. During the next 2 min the black hole remained about stationary near the position of T3, while features in the area of high-reflectivity gradient just south of the 30 n mi (56 km) range mark rapidly moved east-northeast. If the motion of these echo features can be assumed to be predominantly due to horizontal airflow rather than the development or vertical translation of reflecting hydrometeors, then this motion is evidence of appreciable cyclonic relative vorticity centered near U.S. Highway 30 south of the rain-gage network, well south of cyclonic T2 and anticyclonic T3.

At and after 2100 the radar echo exhibits high reflectivity and little detail in the vicinity of the earlier BWER (no scope photos are available 2054–2100). A strong reflectivity gradient is present on the southwest edge (rear flank with respect to direction of storm motion) of the echo, 2100–2104 GMT (Fig. 5). T2 was located on the high-reflectivity edge of this gradient. After 2104 the radarscope photography was at 125 n mi (231 km) range and was of poorer quality. The radar echo continued to move northeast at a slightly increased speed, but no additional hooks, appendages, BWER's or other distinctive features appeared.

T2 was composed of multiple funnels and exhibited rapidly changing form during the first 4 min of its life. Subsequently, only one main funnel was observed, although several small short-lived funnels or vortices exterior but close to the main funnel were seen between 2027 and 2055 (Brown).[2] In contrast to T1, marked horizontal asymmetries were a persistent feature of T2's appearance during most of its photographed life.

Identifiers on Fig. 8 denote location of eyewitnesses or photographers or locations of important features of T2's (and T3's) history as revealed by photographs and movies or as noted by eyewitnesses. T2's intensity apparently increased steadily between 2030 and 2045. The condensation funnel also enlarged during this time, except for two

FIG. 9. Photo taken by Holly Filson (location HF, Fig. 8) of T2 near point C (Fig. 8).

rapid fluctuations occurring near points A and B (Fig. 8). These are cited as possible examples of vortex breakdown by Burggraf and Foster (1977). Fig. 9 is a copy of a photo taken by H. Filson from point HF when T2 was at point C (Fig. 8) and near its greatest intensity. T2 traveled at an average speed of 12 m s^{-1} between Luther and Jordan and slowly decelerated to a near halt at the cusp just before 2100.

The information we have obtained concerning T3 is insufficient to determine its time and place of origin with certainty. Results of our damage survey and the reports of eyewitnesses east of T2's damage track and south of where T3's damage track became well defined are summarized on Fig. 10.

Eyewitnesses at locations RS, HK and J1 on Fig. 10 described strong winds, a "whirlwind" or dust whirl near their location as they were watching T2 to the northwest. Nearly all farms on a 0.5–1 km wide track extending from a garage under construction at location GW northeast to U.S. Highway 30 and then north to the hay field (2 km south of County Road E 26) sustained light damage. In addition, south of U.S. 30 and north of GW, isolated light damage (damage patterns suggesting wind with a westerly component) extends west to T2's damage path.

The sense of rotation of damaging winds that occurred south of the hayfield (where drift marks clearly suggest anticyclonic flow) is uncertain. The occurrence of damaging winds from the south or southwest (as suggested) by damage and reported by eyewitness J. Flynn at location J1) is consistent with motion of a vortex toward the north and northeast, be it cyclonic or anticyclonic. In view of the spatial and temporal continuity of the damage and the eyewitness observations, we believe it most likely that T3 formed as a debris whirl near location GW at about 1436 CST (based on its position relative to T2) and traveled northeast, then north, as a continuous entity until a condensation funnel began to form near location WC (Figs. 8 and 10).

Based on their independent survey and analysis, Fujita[3] and Fujita and Forbes (1979, personal communication) concluded that a small cyclonic tornado formed west of T2 when it was near U.S. Highway 30. It looped cyclonically around T2 on the track shown by the dot-dashed line on Fig. 10. This better accounts for spotty west wind damage which occurred east of T2 along an east-west gravel road 1.5 km south of U.S. 30 than the earlier beginning of T3 that we propose. It is their view that it also better explains the structure of vortex marks they discovered in fields just south of U.S. 30. It does not, however, account for the damage or eyewitness observations south and southwest of location DG, nor does it readily allow for the light damage to outbuildings at location J2.

A frame from the Barthold movie taken about 2044 GMT shows a bowl-shaped, lowered cloud base probably located near the intersection of the damage shown on Fig. 10 with U.S. Highway 30. Several other photos taken of T2 before 2050 which should have had T3 (or, alternatively, the cyclonic tornado proposed by Fujita and Forbes) in the field of view show no cloud or surface debris features that can positively be identified as being associated with an additional tornado. The Barthold movie and photos taken by S. Schneider indicate that near WC (Figs. 8 and 10) T3 began to rapidly intensify as its debris whirl decreased in size. Tornado 3 briefly attained minimal F3 intensity at about 2055 GMT and re-

mained at least F2 intensity until after reaching the cusp in its track.

b. Events after 2100 GMT

Events after 2100 are less well documented than at earlier times. The following summarizes the principal events and briefly discusses possible alternate scenarios. A more complete discussion is given in Brown.[2]

The final photo documentation of the tornadoes is provided by 1) a set of stills taken from near the intersection of county roads R 50 and E 23 (Fig. 8) when T2 and T3 were near their cusps and 2) two scenes from the Barthold movie, shot from location CB on Fig. 8, showing T3 as it passed just south of this location. The stills show that T2 became very wide and diffuse in appearance at its cusp, looking more like a black cloud based at the surface than a tornado. This may be partly due to its being engulfed by heavy rain. This sequence also shows that while

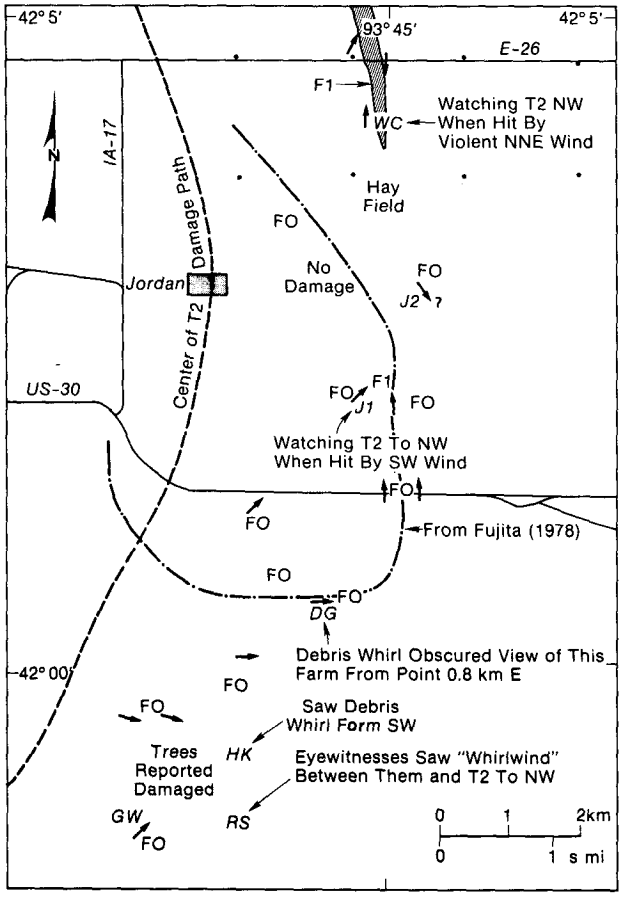

FIG. 10. Eyewitness reports and damage-survey information relevant to T3's early history. Two-letter identifiers mark locations of eyewitnesses or damage. Bold arrows indicate direction of strong wind as inferred from damage patterns. The hatched area north of the "hay field" encloses F1 or greater damage due to T3.

FIG. 11. Frame from Barthold movie shot from location CB showing T3 near point D (Fig. 8).

T3 was at its cusp its funnel at cloud base narrowed and began to move with a *southward* component. By the end of this sequence, T3 was almost a rope, *with a definite southward component to its tilt*. The final scene of the Barthold film began at about this time and shows T3 in a rope formation (Fig. 11), the funnel intersection with cloud base being south of its surface position.

These events seem to eliminate a downdraft deflection as the cause for T3's sharp right turn, as was suggested by Fujita (1977) and observed for waterspouts by Golden (1974). Downdraft outflow is generally found to be strongest within a few hundred meters of the surface as shown by observations (Goff, 1976) and numerical experiments (Mitchell and Hovermale, 1977).

The rain-gage traces provided additional evidence for the complexity of events after 2100. High-wind speeds resulted in high-frequency fluctuations on the rain-gage charts, presumably through vibration of the gage housing and also due to wind-induced pressure fluctuations inside the gage housing. Examination of the traces on days with wind speeds of $\sim$10 m s^{-1} reveals considerable variability between gages in the response to a given wind. Although it might be supposed that the response of a particular gage is approximately proportional to the square of the wind speed, this was not confirmed.

The rain-gage charts were examined carefully for wind-induced fluctuations. High-wind events at each gage were then assigned a number proportional to the log-amplitude of the maximum fluctuation. Fig. 12 summarizes this for all gages. To the right of each gage location on Fig. 12 are times and log-amplitudes (arbitrary scale) of the major high-wind events at that location. Nearly all times on this figure are believed accurate to $\pm$1–2 min (Section 2). An amplitude of 2 is believed to indicate a wind of near or less than 15–20 m s^{-1}. On the basis of damage at nearby locations a wind sufficient to knock the

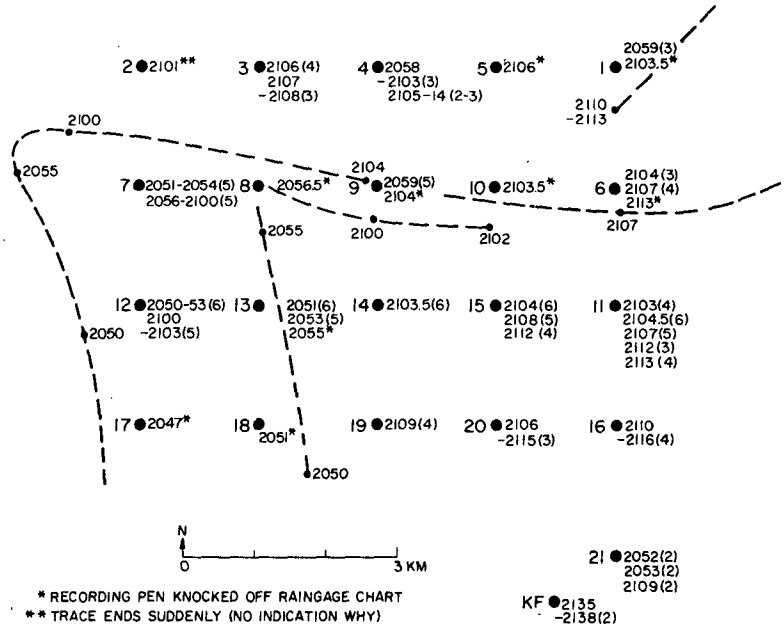

FIG. 12. High-wind events at rain gages. The location of each gage is indicated by a dark circle. The gage number is immediately to the left of each circle. To the right of each circle are the times (GMT) of noteworthy peaks in the wind. In parentheses after each time is a number proportional to the log amplitude of the fluctuation. The dashed lines are the tracks of T2, T3 and T4.

recording pen off the chart (thus disabling the gage) or to produce a fluctuation of amplitude scale 6 (at least one-third of the width of ~15 cm wide chart) is judged to have peaked to at least 35–40 m s^{-1}.

It appears from the figure that high-wind events up to about 2100 GMT were associated with the tornadoes traveling the dashed trajectories shown on the figure. However, high winds appear to have become much more widespread just after 2100, with four of the eight gages in the second and third rows still in operation at 2100 indicating winds of amplitude 6 or greater between 2100 and 2105. Gages 7 and 12 recorded amplitude 5 winds near 2100. In addition, gage 1 in the top row was knocked out at 2103.5 and gage 5 at 2106. The southern part of the gage network experienced weaker winds a few minutes later. The near simultaneous occurrence of strong winds over such a wide area is not readily explained by passage of tornadoes 2 and 3 alone. Because the height of the maelstrom in the north part of the network occurred about 2104, we refer to this as the 2104 event.

Eyewitness tornado and funnel-cloud sightings are inconclusive concerning specific events after 2100 (see Brown).[2] Sightings (to the west) of two or more funnels or tornadoes at one time were reported by a number of observers in the Gilbert vicinity, although the time of these observations is uncertain. Several observers between Gilbert and Ames [notably MX (meteorologist), JT and KB (locations on Fig. 8)] reported seeing one or more funnels aloft near or a little south of Gilbert.

Fig 13 summarizes information pertaining to wind and damage, as gleaned from questionnaires, personal interviews and our damage survey (see Brown[2] for details). On this figure directions of strong or damaging winds (when known with some confidence) are indicated by arrows. Two arrows, separated by commas and enclosed in parentheses, indicate two periods of strong winds. Question marks indicate uncertainty in direction of damaging wind and *V* (variable) indicates damaging winds came from several directions (e.g., near location EB). F isopleths are approximate and do not reflect all apparent local variations in damage intensity.

Space does not allow consideration of all events summarized in Fig. 13 (for detailed discussion, consult Brown[2]). The great complexity of events indicated by the rain-gage network (Fig. 12) is also in evidence here. If we may infer wind direction from damage patterns, strong or damaging winds in the area of F1 or greater damage most often had a westerly component, although all other directions are represented. Many eyewitnesses (locations DB, DK, WH, SN and LJ on Fig. 8) reported two brief periods of strong or damaging winds; this is generally confirmed by the rain-gage records and we believe is further evidence of the 2104 event. Most of the strong or damaging wind at locations south and east of Gilbert was from the southeast to east.

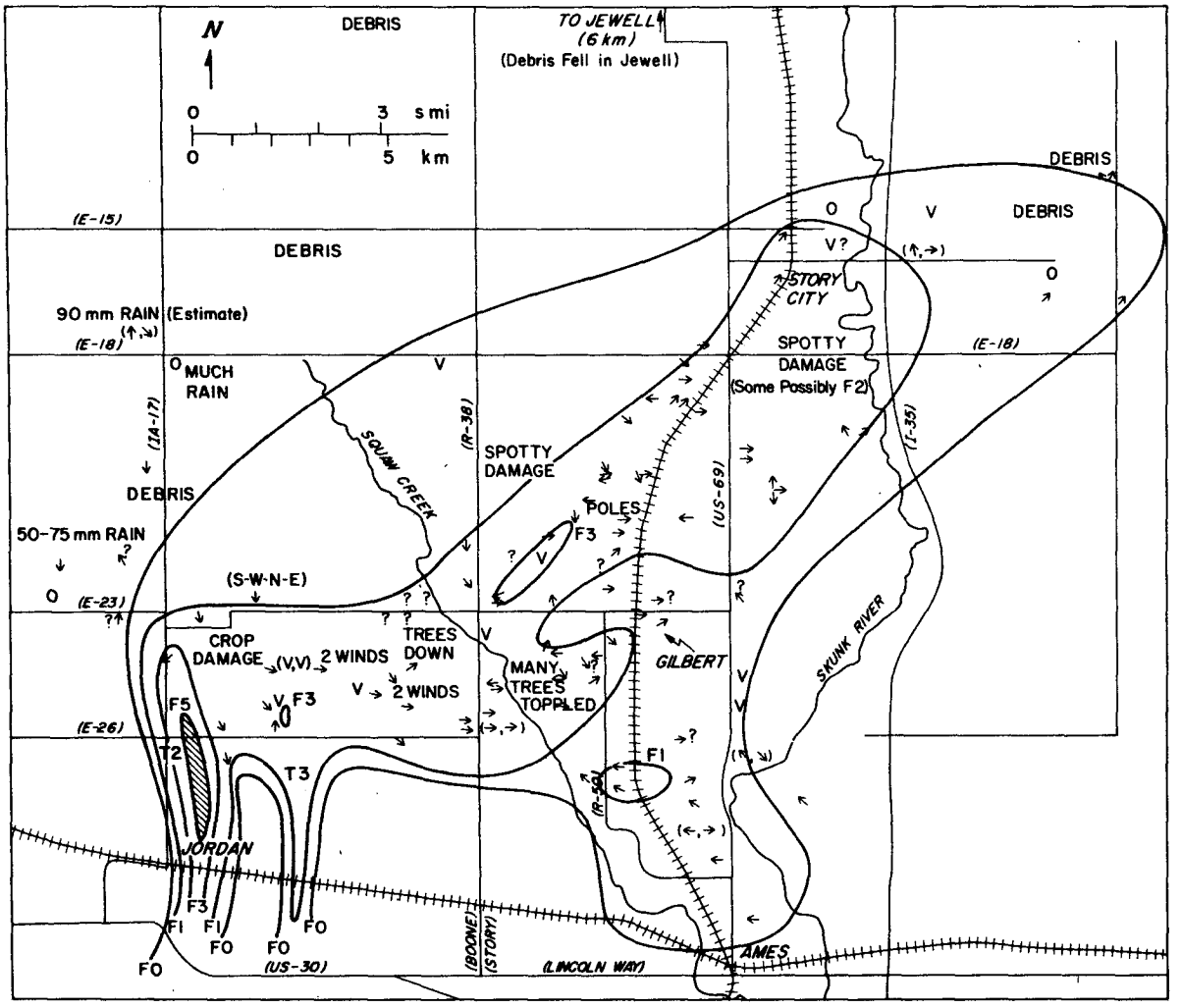

FIG. 13. Summary of damage near, east and north from the cusps in the tracks of T2 and T3. Isopleths are of F-damage scale and may not reflect local variations. Arrows denote directions of strong wind, either observed by eyewitnesses or as suggested by damage. V indicates no preferred direction of strong or damaging wind. (,) indicates two periods of strong wind observed. The question mark by an arrow indicates direction questionable. The question mark standing alone indicates strong wind, direction unknown. 0 indicates no strong wind observed. "Debris" indicates regions well removed from tornado tracks or areas of strong wind where debris from structures was observed to have fallen.

We have been unable to reconstruct with certainty exactly what happened after 2100 GMT. Because of the complex damage patterns, the main questions concern the tracks and times of dissipation of T2 and T3 and time of origin and the nature of T4. The most likely scenario is as follows. About 2100 GMT a narrow finger of very strong north-northwest winds (a "microburst" according to Fujita[3]) destroyed a barn at location RT (Fig. 8) and was probably also responsible for the strong winds at gages 7 and 12. (The sequence of stills taken from the intersection of county roads R 50 and E 23 just before 2100 show a low-level cloud of debris, soil or precipitation advancing swiftly southward from the vicinity of T2. This feature is also visible on the right portion of Fig. 11.) T3 dissipated, as Fujita (1977, and footnote 3) and Fujita and Forbes (1979, personal communication) have indicated, ~5 min after making its right turn. T2 evidently remained in the vicinity of the cusp in its track for ~2–3 min. It then accelerated eastward, but in a weakened state, inflicting F2 damage at location SN (Fig. 8) about 2104 GMT. Between locations DB and DK a well-defined damage path was absent, but damage was extensive in a wooded area near point DK extending to just south of Gilbert. Several eyewitnesses in the Gilbert vicinity observed a ropelike funnel which dissipated south of Gilbert. This timing implies that T2 would have experienced the strong winds of the 2104 event. Such an interaction may explain the lack of a definable damage path between points DB and DK.

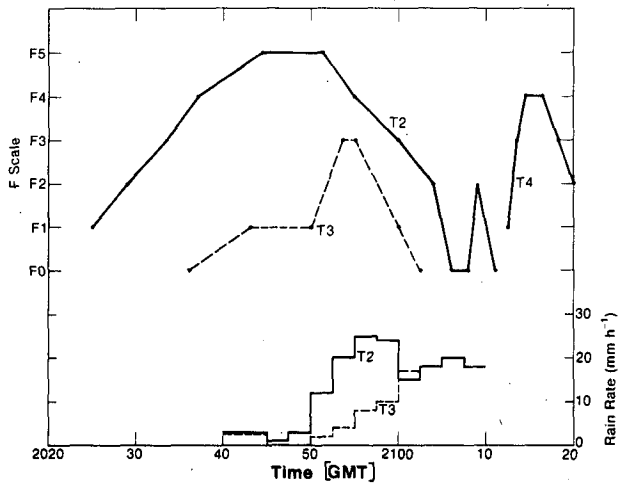

FIG. 14. F-scale intensity for T2, T3 and T4 and rainrates near T2 and T3. Lines pertaining to T2 and T4 are solid, T3 dashed. Rainrates are 2.5 min means along the tornado paths derived by interpretation or extrapolation from the raingage-network observations.

According to this scenario, rain gage 9 experienced some strong winds from T3 at 2059 and was disabled by T2 or the 2104 event strong winds (or a combination). Rain gages 1 and 10 were also disabled by the 2104 event winds and gage 6 experienced them also, but with lesser intensity. The strong winds at 2107 at gage 6 are attributed to T2.

Within a few minutes of T2's demise, a new vortex (T4) evidently rapidly intensified near the intersection of county roads E 23 and R 58 and inflicted a relatively wide swath of F3–F4 damage northwest of Gilbert. [The time of this event may be given by the disabling of gage 6 (Fig. 12) at 2113).] Because the 2104 event also inflicted damage in this area a few minutes earlier, overall damage patterns were complex. [We consider this damage to be tornadic rather than a downburst (Fujita[3]) because severe damage appeared to have occurred from winds of various directions. In addition, Lester Johnson at location LJ recovered checks which fell from the sky 100 km northeast; similar recoveries were reported by persons whose houses were destroyed by T2 south of its cusp and a substantial updraft would seem necessary to explain this phenomenon.]

T4 evidently weakened rapidly northeast of locations EB and JS (Fig. 8) as its circulation expanded. It moved northeast toward Story City at $\sim$12 m s^{-1} as a surface-based tornado cyclone having embedded intense short-lived vortices, or downbursts (Fujita[3]), as suggested by spotty areas of more intense damage. T4 reached Story City about 2125–2130, dissipating shortly thereafter. The extent of the circulation is substantiated by the widespread damage patterns (Fig. 13) and eyewitness reports. (One eyewitness driving south on US 69 encountered strong and sustained headwinds for a distance of 3–4 km.) Similar patterns of widespread damage have been reported by Barnes (1978c) and Brown *et al.* (1973).

5. Discussion

a. Rainfall in relation to tornadoes

The rain-gage network experienced two periods of heavy rain. For both periods, rainfall was heavier and of longer duration over the north and northwest part of the network than elsewhere. Between these two heavy rainfall episodes a period of negligible rainfall was recorded by all the gages in the southeast half of the network during the 2045–2055 GMT interval. This appears to have been associated with the bounded weak echo region (Fig. 5) over the rain-gage network.

Fig. 14 shows the rainfall rate (averaged over 2.5 min intervals) in the immediate vicinity of each tornado as estimated from nearby gages (tracks are those of Fig. 3). The approximate F scale intensity as a function of time is also shown. For the first 15–20 min of its life, T2 was located outside and south of significant rain. However, both T2 and T3 appeared to travel relatively faster than the rain area to their north, and the distance between the tornadoes and the heavy rain decreased with time. Soon after T2 reached the southwest corner of the rain-gage network it began to encounter significant rainfall and for the 5 min or so before reaching its cusp was embedded within rainfall of at least 20 mm h^{-1}. The existence of heavy rain surrounding T2 is verified by photographs taken during this period. Moreover, Fig. 5 shows that T2 was underneath relatively high radar reflectivity after about 2045. After making its turn, T2 remained within rainfall of 15–20 mm h^{-1} until its dissipation. T3, on the other hand, remained free of substantial rainfall until about 2055. Thereafter, it was associated with rainfall of at least 10 mm h^{-1} until it dissipated. Rainfall patterns adjacent to T4 are less certain because of its location outside the rain-gage network. Eyewitness observations indicate that it was associated with relatively heavy precipitation while traveling from north of Gilbert to Story City.

Because of the tremendous potential instability (Fig. 2a), the $\leq$10 m s^{-1} terminal fallspeed of raindrops would have precluded heavy rainfall at the surface underneath a major updraft of the parent thunderstorm. [The strength of the updrafts is substantiated by the *size* (lumber, including $\sim$1 m^2 plywood sheets and two by fours, sheet-metal roofing, even a report of a refrigerator door) of debris scattered over the region north and northeast of the tornado paths (see Fig. 13).] It is therefore concluded that the upward motion within T2's tornado cyclone weakened after 2045–2050, allowing pre-

cipitation to fall to the surface in T2's vicinity. The weakening of the updraft implies weakening of the convergence below it and therefore less concentration of vorticity at lower levels. The encounter with heavy rain as T2 approached its cusp is thus viewed as being intimately connected with T2's subsequent rapid weakening.

The behavior of T3 is also consistent with this picture. Lack of significant surface rainfall and the striking BWER above and near T3 over the period 2048–2054, (Fig. 5) provides evidence for strong upward motion above T3 until slightly before the time of its peak intensity about 2055. Thereafter T3 weakened as it also encountered heavier rainfall.

b. Track structure

The resemblance of the tracks of T2 and T3 (Fig. 3) to a cycloid is intriguing in its implication for the relationship between the tornadoes and storm motions of larger scale. The comparison of T2's path to a cycloid (curtate cycloid, $V_T > \omega a$) is shown in Fig. 15. The cycloidal parameters are given in Table 2. Fig. 15 also compares the translational speeds calculated from movie films to the speeds obtained from this cycloid's parameters. This figure indicates that T2's speed distribution and damage track match a cycloid's speed distribution and track with fairly good approximation.

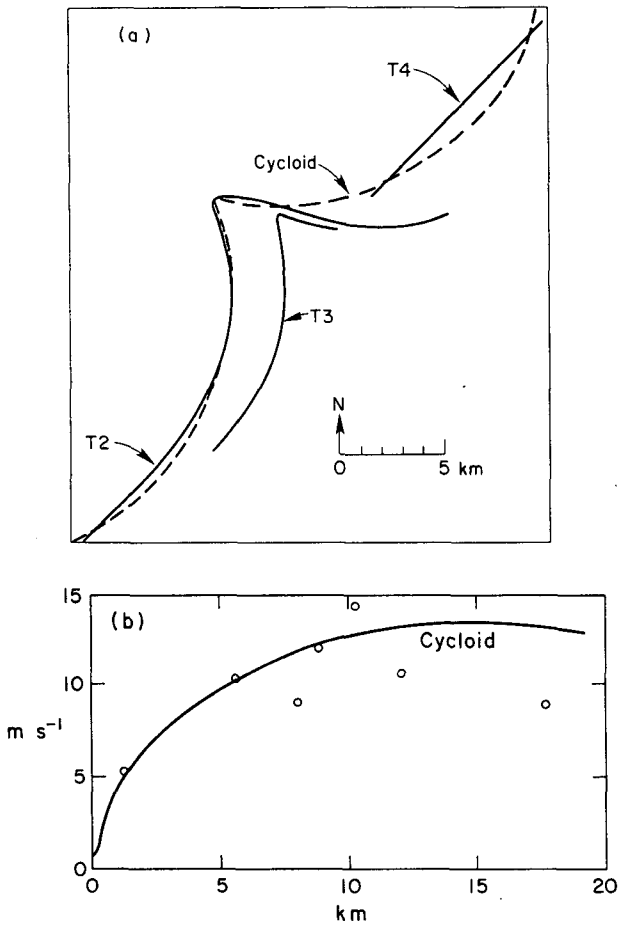

FIG. 15. Comparison of T2's path (a) and translational speed (b) to that of a cycloid with parameters given in Table 2. In (b), s is measured southward with the zero point at the cusp.

TABLE 2. Parameters of cycloid in Fig. 15.

ω (h^{-1})	Radius a (km)	Speed V_T (m s^{-1})
6.5	3.47	7.1

Horizontal trajectories of air parcels embedded in a flow of pure steady rotation with uniform translation superimposed would be cycloidal, with the centerlines of all such trajectories coincident. Furthermore, as discussed by Ward (1972) and Church *et al.* (1979), vortex breakdown may lead to multiple vortices embedded within the parent tornado circulation field based primarily on a function of critical swirl ratio. Agee *et al.* (1976) introduced and applied this concept to the tornado cyclones and the tracks of seven tornadoes in three of the 3 April 1974 tornado families to conclude that the parent circulations associated with each tornado were rotating cyclonically around a common center in response to a translating cyclonic circulation of larger scale. In order to apply this argument here one must assume that the rotation axis of the northeastward-moving parent cyclonic circulation leaned and that the motion of T2 and T3 was governed by flow at separate levels within this circulation.

These necessary modifications to the argument are not readily defended from a fluid dynamical viewpoint. Moreover, there is evidence (especially Fig. 5) that the parent thunderstorm was notably unsteady. We thus prefer an alternative explanation for the tracks of T2 and T3.

c. Surface winds and mesolow

As part of our attempt to examine the formation of T3, we reconstructed the meso-γ scale surface wind field surrounding T2. Since no recording anemometer data were available, we resorted to examination of all still photographs and movies taken of T2 and T3 for evidence of wind effects on trees, grass, bushes, corn, etc., in the foreground of the photos. Each of us independently estimated wind speed and direction for each usable photograph. These "observations" were put into two categories, those with direction uncertainty $\pm$ 45° and those with direction uncertainty $\pm$ 22.5°. In addition, we used wind estimates provided by W. H. Curvin (WC, Figs. 8, 10 and 16) and Terry

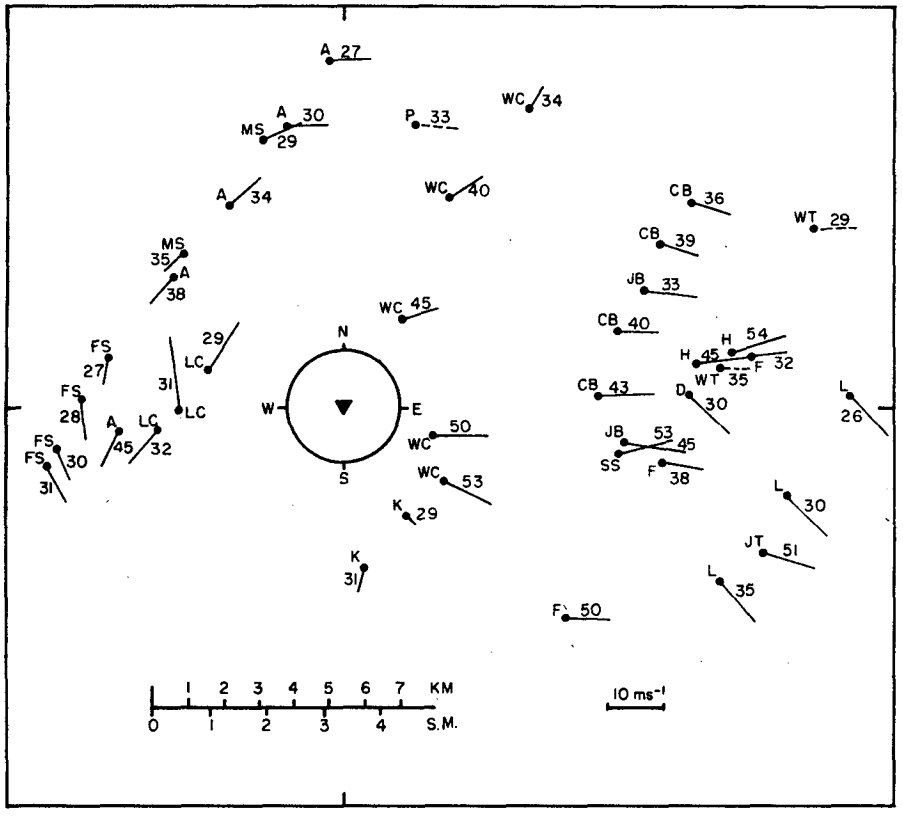

FIG. 16. Earth-relative winds inferred from photographs of T2 and T3 and composited with respect to T2. T2 is at triangle, each photo location is indicated by a dot, and the line emanating from each dot is directed into the wind. The length of each line is proportional to the estimated wind speed. Letters near dots identify the photographer and numbers along each line indicate the time of the photo, in minutes past 2000 GMT. Dashed winds are less reliable.

Legvold (L, Fig. 16). Each observation was then positioned with respect to the center of T2, but without first subtracting T2's motion vector; the result is Fig. 16.

We note that the flow is broadly cyclonic, as we might expect for winds surrounding a major cyclonic tornado. The flow is by no means circularly symmetric, however. Three photographers (A, LC and MS) in the western semicircle provided evidence for a sharp wind shift from northeast to southwest as T2 passed to their east or southeast, and the composite view suggests an asymptote of confluence in the streamline field. In addition, as time passes, wind direction in the eastern semicircle appears to back. The composited winds *relative* to the moving tornado (obtained by subtracting T2's time-varying motion vector from each estimated wind of Fig. 16) appear to exhibit no systematic direction change with time, indicating that the left-turning, decelerating tendency of T2 was probably closely tied to the backing of the surface airflow to its east.

This systematic turning of the airflow can only be explained by the storm-related horizontal pressure gradient force. This could occur through action of a pressure gradient aloft followed by descent to the surface of the air so affected, or by action of a pressure gradient on airflow which remained near the surface. Evidence favors the latter alternative.

Microbarograph records are available from locations KF (29 hour clock), CH and JB (8 day clock) on Fig. 8, and a hygrothermograph record from location KF. The KF records are reproduced in Fig. 17, which shows a major pressure minimum near the time of closest tornado approach. The pressure traces at JB and KF are surprisingly nearly identical, with the minimum pressure at CH being ~1 mb lower (a clock malfunction prevented us from knowing exactly when this occurred). The meso-β scale of this feature suggested by these observations is verified by examination of the microbarograph traces for first- and second-order reporting stations in or adjacent to Iowa. These show that the meso-α scale pressure falls over Iowa were ~2–3 mb between 1900–2100 GMT. DSM, ~60 km south, observed a 5 mb pressure fall and experienced

freshening of the surface southerly flow during this period, indicating a more rapid pressure fall to the north. For a system of this scale the pressure decrease with height is quasi-static, and this large a pressure disturbance with no evidence for a corresponding area of anomalously warm surface temperatures (see KF temperature trace, Fig. 17) justifies the assumption that the mesolow and its associated flow perturbation likely extended through a large depth of the troposphere. It is therefore hypothesized that the mesolow induced horizontal velocity changes of storm scale through a deep layer, and that the deceleration and slow left turn of T2 and T3 and the backing of surface winds east of T2 (Fig. 16) were manifestations of these. To be consistent with these velocity changes, the mesolow must have been centered south of T2 after 2030. The very rapid 25 m s^{-1} east-northeast motion of the small echo which merged with the main storm about 2040–2045 (Fig. 5) may be further evidence of a flow perturbation associated with this mesolow.

There is no evidence to indicate that this mesolow preceded the convection. Rather, it was probably induced by the intense convective activity, although the dynamic processes involved are obscure.

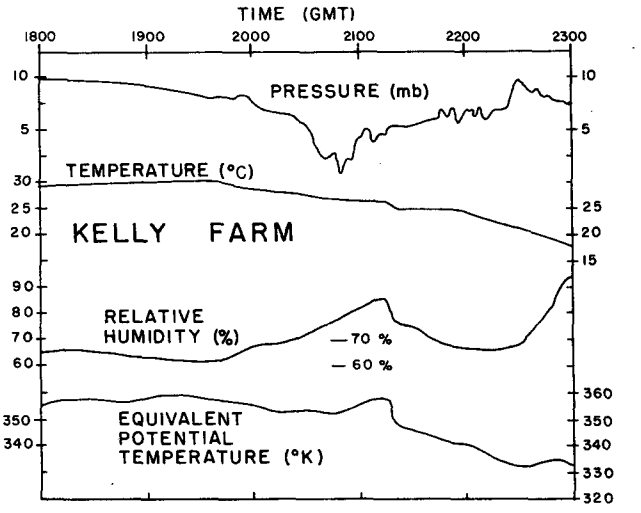

FIG. 17. Microbarograph (approximate sea level pressure in excess of 1000 mb) and hygrothermograph traces from location KF on Figs. 8 and 12. Equivalent potential temperature is derived from the other three measurements, the pressure used being station pressure.

d. Synthesis

A simple, elegant synthesis of the structure of the parent thunderstorm is not possible. This storm does resemble the conceptual supercell model of Browning (1964) in the location of updrafts and heavy precipitation relative to the environmental wind hodograph. However, it is unsteady, with a complex inflow and updraft evolution.

What is known of the storm's early history is summarized in Section 4a. Fig. 18 contains schematics of storm structure at three times while the major cyclonic tornado (T2) was on the ground. The transition 1 (Fig. 4) echo outline and regions of heavy rain ($\geq$20 mm h^{-1}, designated R+) and hail (designated as A) are indicated, along with the locations of T2 and T3. Also shown are *storm relative* surface streamlines (assuming storm motion shown in Fig. 2b), based where possible on the winds plotted in Fig. 16.

We consider it likely that T2's tornado cyclone was associated with the predominant updraft from before the appearance of T2's antecedent wall cloud until the disappearance of the BWER after 2035 GMT. Heavy precipitation and downdrafts were well north of this updraft. After 2000 the mesolow intensified (Fig. 17) with lowest pressure somewhere south of T2 by 2030. The backing of the surface winds east of T2 depicted on Fig. 16 suggests that surface convergence and new updrafts (Fig. 18) developed in response to the mesolow, although there is only indirect evidence for this. Radar reflectivity and surface rainfall patterns, discussed in Sections 4a and 5a, indicate that T2 moved into a region of heavy precipitation after ~2050 GMT, with little or no precipitation to its south or southeast. This is consistent with rain or hail having fallen from a strong updraft to the south into a weakening updraft within T2's tornado cyclone. Photos taken of T2 looking south or southeast show a mostly smooth, well defined base (at $\leq$1 km above ground) to the overcast cloud cover extending south and southeast 5–10 km beyond the edge of T2's wall cloud. Such cloud-base appearance is typical of updrafts (Marwitz *et al.* 1972). The westward-flowing air near the surface east of T2 had θ_E values typical of the prestorm mixed layer, being cooler but more moist, suggesting that this air had experienced isobaric evaporation. It was therefore still capable of sustaining a vigorous updraft. There is no evidence for the existence of a gust front, marking the advancing edge of cool downdraft air, east, south or southwest of T2 before 2045. (Fig. 17 indicates that low-θ_E downdraft air did not reach Kelly Farm until 2115.)

Fig. 19 depicts smoothed streamlines of the surface flow *relative* to T2. These are based on the observations plotted in Fig. 16 with T2's (time varying) motion vector subtracted. In constructing Fig. 19 we have acknowledged the presence of T2 but have ignored T3, which first was observed no earlier than about 2036 GMT. There is no reasonable choice but to indicate *anticyclonic* (negative) streamline curvature to the south and southeast of T2, owing to the east to northeast flow east of T2. The horizontal shear of the surface wind also contributed

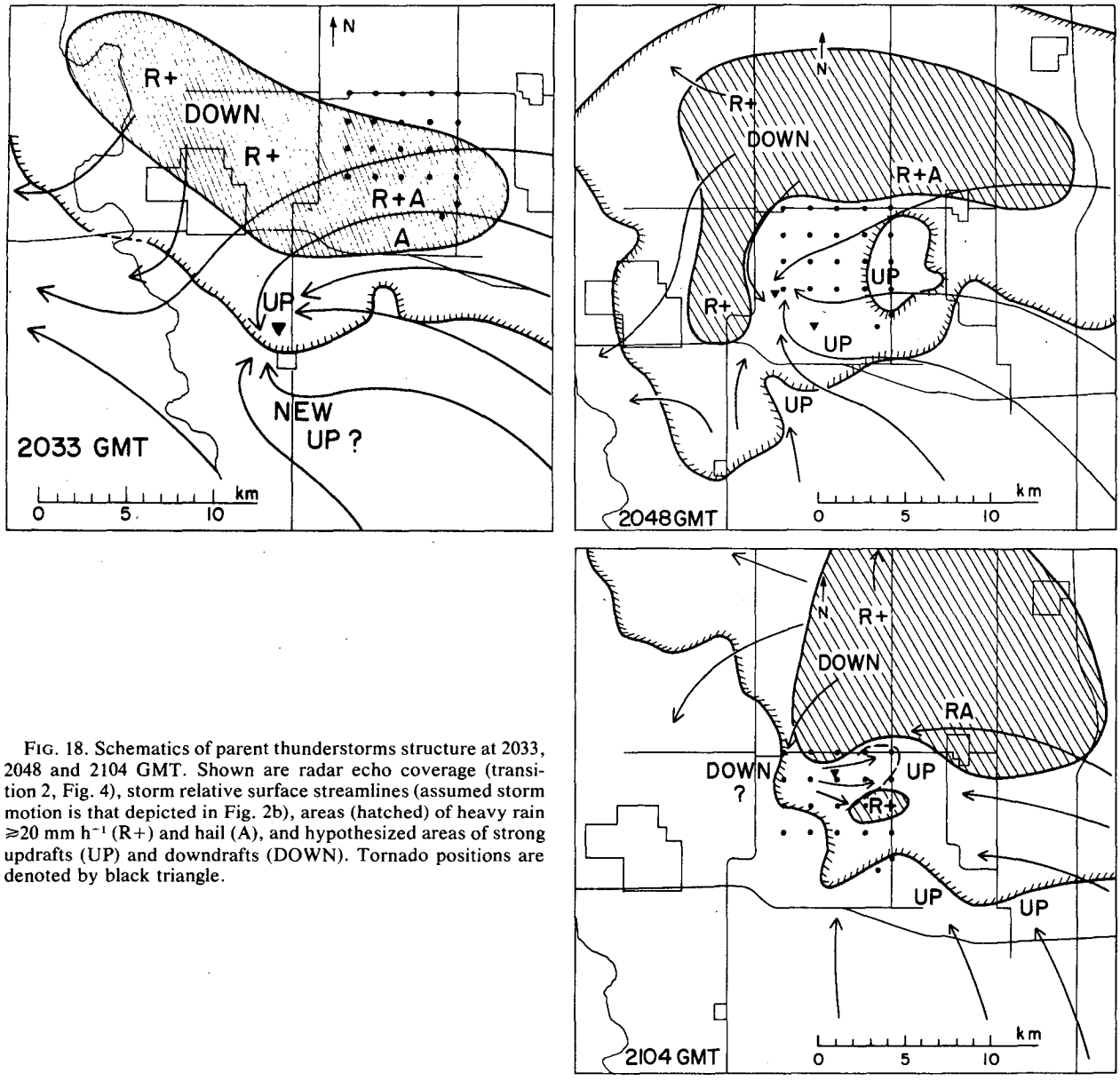

FIG. 18. Schematics of parent thunderstorms structure at 2033, 2048 and 2104 GMT. Shown are radar echo coverage (transition 2, Fig. 4), storm relative surface streamlines (assumed storm motion is that depicted in Fig. 2b), areas (hatched) of heavy rain ≥ 20 mm h^{-1} (R+) and hail (A), and hypothesized areas of strong updrafts (UP) and downdrafts (DOWN). Tornado positions are denoted by black triangle.

to a negative value for the vertical component of vorticity south and southeast of T2. That the anticyclonic tornado formed in this region argues that horizontal convergence resulted in vertical stretching of the low-level anticyclonic vortex tubes.

What was the source of this anticyclonic vorticity? On the basis of the appearance of low-level cloud fragments southeast of T2 along the edge of T2's wall cloud, and in consideration of the prestorm wind hodograph (Fig. 2b) it is likely that the southerly and westerly component of the low-level airflow increased rapidly with height within a few kilometers south and east of T2. Vortex lines probably pointed toward the northwest quandrant in this region. An updraft centered at low levels 5–10 km south of T2 would have tended to tilt those vortex lines into the vertical such that the vertical component of vorticity would have become negative. This is illustrated in Fig. 20 as viewed from above; quasi-horizontal vortex lines (A) are tilted toward the vertical and stretched (B and C) as they move westward relative to T2, resulting in a column of anticyclonic vorticity. (Although the tilting process does not formally operate at a level ground surface, it is effective a few hundred meters above. The appearance of appreciable anticyclonic vorticity very near the surface can be accounted for by downward diffusion of this vorticity and its am-

plification by horizontal convergence at low levels.) The crucial aspect of this process is the development of the updraft south of T2, initiated by convergence due to the mesolow.

The cyclonic rotation of radar echo features, observed 2051–2053 GMT, (Fig. 5) and centered south of the rain-gage network and tornadoes, may be evidence for rotation of opposite sign generated by tilting and stretching of vortex tubes on the opposite (southern) side of this updraft. The rotation may thus be analogous to the rotation in echo features near and before T2's formation (Section 4). No anticyclonic rotation of echo features in the vicinity of T3 is detected.

The 2048 GMT schematic (Fig. 18) shows storm structure when T2 and the mesolow to its south and southeast were near their greatest intensity. We argued above (Section 5a) that heavy rain near T2 beginning about 2050 (Fig. 14) indicates weakening by 2045–2050 of the updraft associated with T2's tornado cyclone, whereas near, south and east of T3 updrafts continued strong. This is consistent with the rapid intensification of T3 between 2050 and 2055. Accordingly, we have placed the locations of major updrafts near the BWER and southwestward across the southeast portion of the raingage network where little rain was falling. On the basis of eyewitness descriptions and photos and from radar indications, heavy rain and hail, along with divergent surface winds, are placed north of the raingage network. Heavy rain was reportedly beginning to obscure views of T2 from Boone at this time.

Following 2050 the pressure at both KF and JB began to rise rapidly. We believe this was associated with filling and northeastward movement of the mesolow; it appears from eyewitness reports that east winds east of T2 in the Ames vicinity reached peak intensity before 2100, with winds becoming light thereafter.

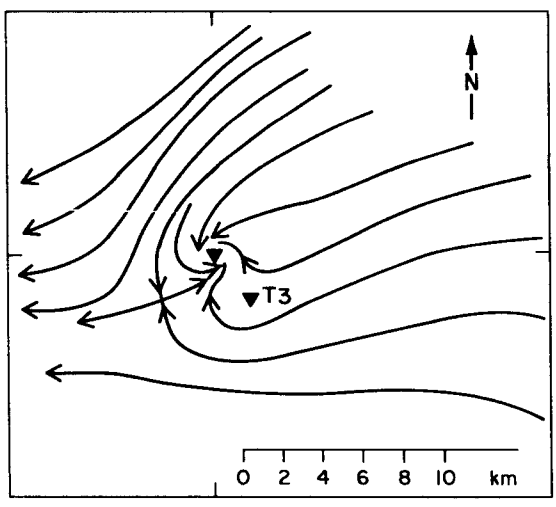

FIG. 19. Smoothed streamlines of the wind field relative to a coordinate system moving with T2 and not rotating with respect to the earth. This streamline pattern is based on the subset of Fig. 16 winds observed between 2026 and 2040. Little change results if one also uses winds observed later.

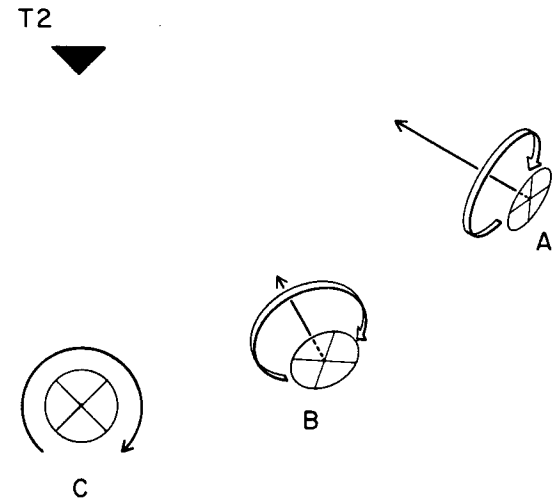

FIG. 20. Schematic illustrating tilting of quasi-horizontal vortex lines into the vertical due to an updraft south of T2. See text.

We earlier presented evidence that the sharp right turn made by T3 was not the result of interaction with air spreading southeastward near the surface from a downdraft to the northwest, as proposed by Fujita (1977). (The evidence concerning T2 is not so clear.) Rather it is hypothesized that the turns made by T2 and T3 may have been the result of motion of the mesolow toward the northeast, such that an eastward or southeastward directed pressure gradient force of storm scale through a deep layer was experienced by the airflow over and near the rain-gage network after ~2045. [Recall that locations JB and KF (Fig. 8) both had their lowest pressures at about 2045.] This eventually resulted in a northwesterly flow component.

Very soon after the tornadoes made their sharp turns a narrow swath of very strong north-northwest winds occurred south of T2. A short time later there followed the 2104 event (Section 4b). The downdraft in the area of heavy rain and hail north of the raingage network (see Fig. 18) is suggested by eyewitness reports of northerly winds accompanying the heavy rain north of the network. Radar indications are that strong updrafts by this time were mainly well south or southeast of the rain-gage network. The 2104 event is represented in Fig. 18 by the westerly flow indicated over the northern portion of the raingage network.

After T2 moved into the region of heavy rain and closer to downdrafts it is hypothesized that descending, negatively buoyant air became entrained into its tornado cyclone circulation from the north or west.

The 2104 event may have resulted from very rapid eastward acceleration of some of this air as it turned cyclonically toward the east and continued to descend, causing it to reach the surface with high westerly momentum. The precise dynamical processes involved are obscure.

Subsequent to 2104 GMT there is very little on which to base estimates of the parent thunderstorm structure. Our hypothesis is that the tornado cyclone earlier associated with T2 may have split after 2104, with one center remaining associated with T2 and the other moving eastward more slowly and subsequently becoming the parent circulation for T4. T4's formation suggests that a substantial updraft resumed after 2104 across the northern part of the raingage network. The short lifetime of severe tornadic winds northwest of Gilbert, the widespread damage (suggestive of a surface-based tornado cyclone) and heavy rain accompanying the widespread damaging winds from north of Gilbert to Story City (Fig. 13) all suggest that upward motion in this area was weak or nonexistent after about 2115.

6. Concluding remarks

Very few well-documented anticyclonic tornadoes have been reported (Fujita, 1977) and probably none have better documentation than this one. According to Burgess (1977, personal communication) most have occurred simultaneously with a (usually) stronger cyclonic tornado. Typical location of the anticyclonic tornado is a few kilometers to the right (with respect to direction of storm motion) of the cyclonic tornado, as in this case.

What was distinctive about this storm that led to an anticyclonic tornado? We approach this question by comparing the structure of our storm to that typical of other tornadic thunderstorms reported in the literature.

Lemon and Doswell (1979) have developed a conceptual model of an "evolving supercell" based on several recent case studies of severe thunderstorms probed by Doppler radar. A prominent aspect of supercell evolution in these cases was the low-level cyclonic sweep of downdraft air from the left rear of the supercell's mesocyclone to its right flank (directions with respect to direction of storm motion). In storms analyzed by Barnes (1978a,b), Golden and Purcell (1978), Lemon *et al.* (1978) and Brandes (1978), tornado development occurred as the gust front, marking the leading edge of the downdraft air, swept around the right flank of the mesocyclone. In cases where Doppler data allowed determination of horizontal flow, the low levels were dominated by mesocyclonic circulation as the gust front rotated around the mesocyclone center. The development of a reflectivity "hook" harboring a WER or BWER was attributed to precipitation advecting cyclonically around the rear flank of the mesocyclone as it intensified at low levels.

Because the Lemon-Doswell (1979) model is based on analysis of only a few storms, its general applicability remains to be determined. It appears, however, that a number of storms analyzed before Doppler radar became available (e.g., Fujita, 1958; Browning and Ludlam, 1962; Browning and Donaldson, 1963; Browning, 1965) may have resembled this model.

The storm under study here, however, appears to be distinctive in important respects. Although the first (cyclonic) tornado T1 had associated with it a lowered cloud base and cloud-band structure similar to that noted by Golden and Purcell (1978, Fig. 8) for the Union City, Oklahoma tornado, a corresponding hook echo and BWER as noted in the Union City storm (Lemon *et al.*, 1978) was not detected and the cloud band was *not* associated with a gust front. In addition, it is concluded that *no gust front penetrated significantly southeast of a line running southwest from the position of T2 from its inception until at least 2100 GMT* (Section 5d).

Surface mesonetwork observations have often revealed meso-γ scale areas of surface low pressure dynamically tied to surface mesocyclones or tornado cyclones in supercell thunderstorms (e.g., Barnes, 1978a,b; Fujita, 1958; Hoxit *et al.*, 1976). *By contrast, the mesolow observed in this storm appears to have been largely unrelated to the main tornado cyclone* (that associated with T2). Furthermore, the mesolow was probably larger in horizontal scale than is typical of mesolows associated with isolated supercell storms. As discussed in Section 5, it was centered south or southeast of the tornadoes before 2045–2050 GMT and was probably responsible for updraft development south of T2.

Taken together, these considerations lead us to offer the following speculation concerning why this storm produced an anticyclonic tornado. Development of updrafts south of a tornado cyclone is commonly observed, typically along the gust front to the right or right rear of the principal mesocyclone or tornado cyclone (direction with respect to overall storm motion). An example is the "flanking line" of Lemon (1976); see also Brandes (1978, Fig. 13). Because of the direction of the vertical wind shear in the environment of such an updraft, vortex-line tilting will produce a cyclonic-anticyclonic vortex couplet within it with the anticyclonic member toward the *cold* side of the gust front (see e.g., Brandes, 1978, Fig. 15). Such a flanking-line updraft, if it is to survive, must feed on the potentially buoyant air rising at the gust front rather than on

the cold air to its rear. This updraft must then remain tied to the gust front and convergence will occur on the side of the updraft where tilting favors cyclonic vorticity. Consequently, vortex-tube stretching will favor the dominance of cyclonic vorticity within the updraft, especially at low levels.

The absence of downdraft air south and east of T2 where new updraft development occurred means that in our storm the updraft could have been sustained by low-level air converging from *either* the right or left flank of the new updraft. Thus, *factors which appear to inhibit development of strong anticyclonic vorticity* in an updraft located to the right of the pre-existing mesocyclone in a more typical severe storm *were absent in this storm*.

Even if one grants that this speculation is valid and that this storm's apparently unusual structure was responsible for the anticyclonic tornado development, there is still the question of *why* the storm took on the unusual structure. The environmental temperature and moisture stratification and wind hodograph (Fig. 2) are qualitatively similar to the environments of other severe storms discussed in the literature. Careful experimentation wih a cloud model such as that of Klemp and Wilhelmson (1978a), which has demonstrated striking success in reproducing the principal features of supercell storms (Klemp and Wilhelmson, 1978b), might provide some insight into this question.

Acknowledgments. This research was partially supported by Grant 01-7-022-13204 from the National Severe Storms Laboratory (NSSL) of NOAA to Iowa State University (ISU). The physical insights of both Bob Davies-Jones and Don Burgess of NSSL were helpful in increasing our comprehension of the data. Davies-Jones also provided us copies of the questionnaire used by NSSL and arranged for the duplication of several movies shot by eyewitnesses.

We acknowledge a very useful and stimulating exchange of ideas concerning this case with Ted Fujita and Greg Forbes. The comments of Ed Zipser and of an anonymous reviewer were also helpful in improving the manuscript. In addition, one of us (JB) had useful discussions with Rich Rotunno and Morris Weisman concerning this case.

We thank Cecilia Griffith for vital assistance in use of the color densitometer at the National Hurricane and Experimental Meteorology Laboratory of NOAA. Harry C. Vaughan of ISU flew a damage-survey mission for us on 15 June 1976. John L. Stanford of ISU provided useful assistance and encouragement. Warren Caldwell, Meteorologist in Charge at NWSFO, Des Moines, provided a copy of the radar log and microbarograph trace for the period covering the storm. John Hales and William C. Henry of the National Severe Storms Forecast Center furnished us with hourly surface observations.

Pete Johnsen, and members of the Graphics Section at NCAR, drafted some of the figures. Mrs. Elaine Ardourel and Mrs. Irene Bork performed the typing.

Finally and most important, we acknowledge the 200 or so individuals and families living in or near the damage-stricken areas who happily responded to our requests for any information they could provide. It was indeed a pleasure to work with these good people of Iowa.

REFERENCES

Agee, E. M., J. T. Snow and P. R. Clare, 1976: Multiple vortex features in the tornado cyclone and the occurrence of tornado families. *Mon. Wea. Rev.*, **104**, 552–563.

Barnes, Stanley L., 1978a: Oklahoma thunderstorms on 29–30 April 1970. Part I: Morphology of a tornadic storm. *Mon. Wea. Rev.*, **106**, 673–684.

——, 1978b: Oklahoma thunderstorms on 29–30 April 1970. Part II: Radar-observed merger of twin hook echoes. *Mon. Wea. Rev.*, **106**, 686–696.

——, 1978c: Oklahoma thunderstorms on 29–30 April 1970. Part III: Tornado characteristics inferred from damage tracks. *Mon. Wea. Rev.*, **106**, 697–703.

Brandes, E. A., 1978: Mesocyclone evolution and tornadogenesis: some observations. *Mon. Wea. Rev.*, **106**, 995–1011.

Brown, Rodger A., Donald W. Burgess and Kenneth C. Crawford, 1973: Twin tornado cyclones within a severe thunderstorm: single Doppler radar observations. *Weatherwise*, **26**, 63–71.

——, Leslie R. Lemon and Donald W. Burgess, 1978: Tornado detection by pulsed Doppler radar. *Mon. Wea. Rev.*, **106**, 29–38.

Browning, K. A., 1964: Airflow and precipitation trajectories within severe local storms which travel to the right of the wind. *J. Atmos. Sci.*, **21**, 634–639.

——, 1965: The evolution of tornadic storms. *J. Atmos. Sci.*, **22**, 664–668.

——, and F. H. Ludlam, 1962: Airflow in convective storms. *Quart. J. Roy. Meteor. Soc.*, **88**, 117–135.

——, and R. J. Donaldson, Jr., 1963: Airflow and structure of a tornadic storm. *J. Atmos. Sci.*, **20**, 533–545.

Burggraf, Odus R., and M. R. Foster, 1977: Continuation or breakdown in tornado-like vortices. *J. Fluid. Mech.*, **80**, 685–703.

Church, C. R., J. T. Snow, G. L. Baker, and E. M. Agee, 1979: Characteristics of tornado-like vortices as a function of swirl ratio: A laboratory investigation. *J. Atmos. Sci.*, **36**, 1755–1776.

Davies-Jones, Robert P., 1978: Tornado dynamics. *Thunderstorms: A Social and Technological Documentary*, E. Kessler, Ed. University of Oklahoma Press.

Fujita, Tetsuya, 1958: Mesoanalysis of the Illinois tornadoes of 9 April 1953. *J. Meteor.*, **15**, 288–296.

——, 1977: Anticyclonic tornadoes. *Weatherwise*, **30**, 51–64.

Goff, R., 1976: Vertical structure of thunderstorm outflows. *Mon. Wea. Rev.*, **104**, 1429–1440.

Golden, J. H., 1974: On the lifecycle of Florida Keys' waterspouts, I. *J. Appl. Meteor.*, **13**, 676–692.

——, and D. Purcell, 1978: Life cycle of the Union City, Oklahoma tornado and comparison with waterspouts. *Mon. Wea. Rev.*, **106**, 3–11.

Hoxit, L. R., C. F. Chappell and J. M. Fritsch, 1976: Formation of mesolows or pressure troughs in advance of cumulonimbus clouds. *Mon. Wea. Rev.*, **104,** 1419–1428.

Johnson, Richard H., 1977: Effects of cumulus convection on the structure and growth of the mixed layer over south Florida. *Mon. Wea. Rev.*, **105,** 713–724.

Klemp, J. B., and R. B. Wilhelmson, 1978a: The simulation of three-dimensional convective storm dynamics. *J. Atmos. Sci.*, **35,** 1070–1096.

——, and ——, 1978b: Simulations of right- and left-moving storms produced through storm splitting. *J. Atmos. Sci.*, **35,** 1097–1110.

Lemon, L. R., 1976: The flanking line, a severe thunderstorm intensification source. *J. Atmos. Sci.*, **33,** 686–694.

—— and C. A. Doswell III, 1979: Severe thunderstorm evolution and mesocyclone structure as related to tornadogenesis. *Mon. Wea. Rev.*, **107,** 1184–1197.

——, D. W. Burgess and R. A. Brown, 1978: Tornadic storm airflow and morphology derived from single-Doppler radar measurements, *Mon. Wea. Rev.*, **106,** 48–61.

Marwitz, John D., 1972: The structure and motion of severe hailstorms. Part I: Supercell storms. *J. Appl. Meteor.*, **11,** 166–179.

——, August H. Auer and Donald L. Veal, 1972: Locating the organized updraft on severe thunderstorms. *J. Appl. Meteor.*, **11,** 236–238.

Mitchell, K. E., and J. B. Hovermale, 1977: A numerical investigation of the severe thunderstorm gust front. *Mon. Wea. Rev.*, **105,** 657–675.

Orlanski, I., 1975: A rational subdivision of scales for atmospheric properties. *Bull. Amer. Meteor. Soc.*, **56,** 527–530.

Ward, Neil B., 1972: The exploration of certain features of tornado dynamics using a laboratory model. *J. Atmos. Sci.*, **29,** 1194–1204.